International Journal of Pharmaceutics 430 (2012) 56–64

Contents lists available at SciVerse ScienceDirect

International Journal of Pharmaceutics

journal homepage: www.elsevier.com/locate/ijpharm

Enhancing crystalline properties of a cardiovascular active pharmaceutical ingredient using a process analytical technology based crystallization feedback control strategy

Ali N. Saleemi [a], Gerry Steele [a], Nicholas I. Pedge [b], Anthony Freeman [a], Zoltan K. Nagy [a,*]

[a] Department of Chemical Engineering, Loughborough University, Loughborough, LE11 3TU, United Kingdom
[b] AstraZeneca, Macclesfield, Cheshire, SK10 5TL, United Kingdom

ARTICLE INFO

Article history:
Received 27 January 2012
Received in revised form 16 March 2012
Accepted 17 March 2012
Available online 24 March 2012

Keywords:
Automated direct nucleation control
Pharmaceutical crystallization
Solvent inclusion

ABSTRACT

Pharmaceutical regulatory bodies require minimal presence of solvent in an active pharmaceutical ingredient (API) after crystallization. From a processing point of view bigger crystals with minimal agglomeration and uniform size distribution are preferred to avoid solvent inclusion and for improved downstream processing. The current work addresses these issues encountered during the production of the potential anti-arrhythmic cardiovascular drug, AZD7009. This paper demonstrates that by applying the automated direct nucleation control (ADNC) approach problems with agglomeration and solvent inclusion were resolved. This model free approach automatically induces temperature cycles in the system, with the number of cycles, temperature range and adaptive heating and cooling rates determined to maintain the number of particles in the system, as measured by a focused beam reflectance measurement (FBRM) probe, within a constant range during the crystallization. The ADNC approach was able to produce larger and more uniform crystals and also removed the residual solvent trapped between the crystals compared to the typical crystallization operation using linear cooling profile. The results illustrate the application of process analytical technologies, such as FBRM and ATR-UV–vis spectroscopy, for the design of optimal crystallization operating conditions for the production of pharmaceuticals, and demonstrate that the ADNC approach can be used for rapid crystallization development for APIs exhibiting problems with agglomeration and solvent inclusion.

1. Introduction

The final step in the production of an active pharmaceutical ingredient (API) is crystallization. However, crystallization of an API is often problematic, since there are many issues to be addressed, e.g. purity, yield, average size, shape and size distribution, polymorphism/crystallinity (Variankaval et al., 2008). From a primary manufacturing perspective these factors can affect, e.g. filtration and drying rates and some of them can also cause problems in secondary manufacture such as batch variation in powder flow properties, particle size reduction and compaction into tablets (Hagsten et al., 2008). Therefore, it is often necessary to understand crystallization processes thoroughly and scientifically define a set of conditions that can be used to manufacture batches reproducibly at progressively larger scales.

Process analytical technology (PAT) is now commonplace in the pharmaceutical industry for the monitoring of reactions and crystallizations because it can provide a wealth of real-time data, especially when used in situ, for process understanding and control (Barrett et al., 2005; Fujiwara et al., 2002). Techniques routinely used include focused beam reflectance measurements (FBRM) for in situ analysis of the evolving crystal size distribution (Kail et al., 2009; Abu Bakar et al., 2010; Barthe and Rousseau, 2006; Doki et al., 2004; Hermanto et al., 2010; Simon and Myerson, 2011; Hishamuddin et al., 2011), and also in-line spectroscopic techniques such as attenuated total reflectance Fourier transformation infrared (ATR-FTIR) and ATR ultraviolet–visible (UV–vis) spectroscopy for solution concentration measurements (Billeter et al., 2008; Borissova et al., 2009; Billot et al., 2010; Aamir et al., 2010a,b; Saleemi et al., 2012a,b,c) or for monitoring polymorphic transformation (Abu Bakar et al., 2011; Howard et al., 2009a,b). In addition, the appearance and growth of crystals can be directly observed in the reactor by way of an in-process visualization aids such as particle vision monitor (PVM) (Jia et al., 2008) or other in situ imaging techniques (Qu et al., 2006; Li et al., 2008; Simon et al., 2009a,b; Simon et al., 2010a,b). In recent years the Food and Drugs Administration (FDA) has advocated the use of PAT in crystallization and have detailed a number of in-line and on-line monitoring techniques (Yu et al., 2004).

* Corresponding author. Tel.: +44 1509 222516; fax: +44 1509 223923.
E-mail address: Z.K.Nagy@lboro.ac.uk (Z.K. Nagy).

0378-5173/$ – see front matter © 2012 Elsevier B.V. All rights reserved.
doi:10.1016/j.ijpharm.2012.03.029

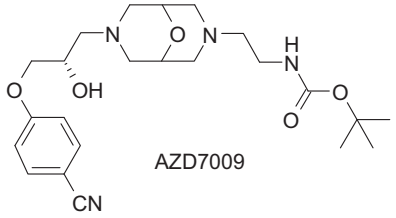

Fig. 1. Structure of AZD7009.

In this paper, the solution to some of the issues encountered with the production of the active pharmaceutical ingredient, AZD7009 (tert-butyl 2-{7-[(2*S*)-3-(4-cyanophenoxy)-2-hydroxypropyl]-9-oxa-3,7-diazabicyclo[3.3.1]non-3-yl}ethylcarbamate (Fig. 1) and the role of PAT in process design are detailed. AZD7009 was nominated as an orally delivered anti-arrhythmic cardiovascular drug (Goldstein et al., 2004).

Owing to the high therapeutic dose of AZD7009, peak sales projections were predicted to be ~300–400 tonnes of API a year at peak scales. From a pharmaceutical perspective this can represent a challenge when developing a batch process for this compound. Earlier work on this compound (which at that time was not explicitly identified for commercial reasons) showed that it had a propensity to oil out (Deneau and Steele, 2005) and more than 100 pure and mixed solvents were screened in an effort to find a system from which it could be crystallized. Eventually this was achieved from a mixture of di-*iso*-propyl ether (DIPE) and *iso*-propanol (IPA) (10:2 DIPE/IPA), which typically gave a >85% recovery from 12 solvent volumes. However, analysis of early batches of the compound showed that although the material was highly crystalline and very pure (99.5%) the API, even after recrystallization, contained residual DIPE at a level of 1500–2000 ppm, resulting in a strong odour which persisted even after drying in a vacuum oven at 55 °C.

The International Committee for Harmonization (ICH) has published a guideline (ICH Q3c) for residual solvents such that drug products should contain levels of residual solvents no higher than can be supported by safety data. The permitted daily exposure (PDE) is defined as the pharmaceutically acceptable intake of residual solvent. The solvents are classified into three classes of which those in the Class III category are the most preferred, since these are the ones with the lowest toxic potential, e.g. acetic acid, acetone, ethanol ethyl acetate and ethyl ether, which have PDEs of 50 mg or more a day. Camarasu et al. (2006) have reported recent progress in the determination of volatile impurities in pharmaceuticals.

The ICH guidelines also define a fourth class of solvents for which no adequate toxicological data on which to base a PDE has been found. DIPE falls into this class and the guideline comments that manufacturers should supply justification for residual levels of solvents. DIPE is also less favoured as solvent because of its propensity to form peroxides on storage, which can cause explosive instability (Hunter and Downing, 1949). Therefore, from a manufacturing and regulatory point of view DIPE was not ideal but, as noted earlier, it was the only solvent that could be used to avoid oiling out and obtain crystalline material. Unfortunately, DIPE has an extremely low odour threshold whereby 100% of subjects can detect 0.1 ppm levels (Smallwood, 2002). Since this level corresponds to ~25 ng in a 250 mg tablet, the residual ether smell made the tablets containing the API difficult to blind for use in clinical trials. The formulation team therefore requested that the DIPE odour be eliminated from future batches of the API. Furthermore, the formulation team also requested larger crystals, which were found to have better flow and compression characteristics when making extended release tablets.

The challenge was therefore to develop a cost-efficient process that produced large crystals of AZD7009 with no residual solvent smell. During development, this was achieved using a typical temperature cycling (ripening) regime post-crystallization. Whilst the classical temperature cycling approach allowed the delivery of 750 kg of AZD7009 to supply Phase II and III clinical trials (Juppo and Steele, 2006), it used a fixed number of cycles within constant upper and lower temperature limits. The crystallization and dissolution of the same amount of crystals in each cycle increased considerably the duration of the batch. The switching between the heating and cooling stages, the heating/cooling rates and number of cycles were determined heuristically, and verified subsequently using economic calculation based on the operating costs of the process. This paper describes a completely automated ripening technique – automated direct nucleation control (ADNC), which provides a rapid and robust design of the necessary temperature cycling procedure to achieve the desired product characteristics with minimal prior knowledge about the system.

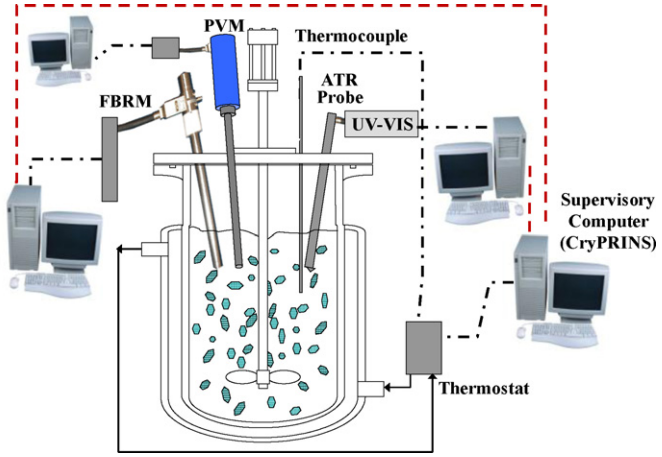

Fig. 2. Experimental setup used for the experiments.

2. Materials and methods

Solvents used in the experiments, namely DIPE (laboratory reagent grade) and IPA (analytical reagent grade), were purchased from Fisher Scientific, Loughborough, UK. Crude AZD7009 with >99% purity was supplied by Development Manufacture, Process R&D, AstraZeneca R&D Charnwood, Loughborough, UK.

The experiments were carried out in a 400 mL jacketed glass vessel fitted with an overhead PTFE coated 4-pitched blade turbine and thermocouple (Fig. 2). The temperature was controlled by a thermo fluid circulator bath (Huber Variostat CC-415 VPC). An FBRM probe (model D600, Lasentec) was used to measure chord length distributions. FBRM data collection and monitoring was carried out by the FBRM control interface software (version 6.7). The UV–vis spectra of the solution were measured using a Hellma 661.822 ATR probe connected to a Carl Zeiss MCS621 UV–vis spectrometer. Software written in LabVIEW (National Instruments) using libraries provided by Carl Zeiss was used for spectra collection. The FBRM, UV–vis and temperature data were recorded every 10 s. The data collected by computers connected to FBRM and UV–vis were sent to a third computer, running the Crystallization Process Informatics System (CryPRINS) software (in-house developed software, available commercially by contacting the corresponding author) written in LabVIEW. This software is capable of receiving and sending data through an RS232 interface, by file sharing, dynamic data exchange (DDE) or using an OPC (OLE – Object Linking and Embedding – for Process Control) server. The CryPRINS software allows real-time communication with a variety of process analytical technology tools (e.g. FBRM, ATR-UV–vis, ATR-FTIR, Raman, conductivity, turbidity, etc.) introducing the concept of

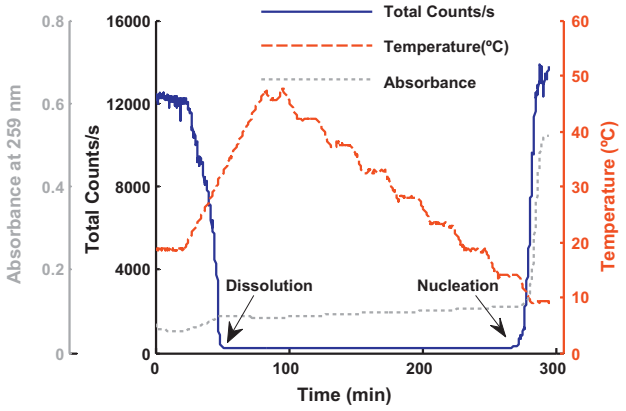

Fig. 3. Calibration experiment carried out at the saturation temperature of 40 °C.

composite PAT array (CPA), whereby signals from different PAT tools are combined and used simultaneously to achieve better and more robust monitoring and control of the crystallisation systems. CryPRINS is the first commercially available software system which provides automated calibration approaches and implements a series of advanced model-free crystallization control approaches (e.g. supersaturation control (SSC), ADNC, combined sequential and simultaneous SSC-ADNC, in situ seed generation, etc.) with advanced temperature tracking and combined cooling/antisolvent operation modes. It also provides a simplified model-based estimation approach for the prediction of the product crystal size distribution at the end of the batch, allowing operators to adjust operating conditions to achieve target product properties. The communication interface offers immediate application of the CryPRINS at both laboratory and industrial scale, a feature which in combination with the advanced feedback control based approaches make CryPRINS an excellent framework as an intelligent decision support system for rapid crystallisation design and scale-up.

Scanning electron microscopy (SEM) was performed using a Quanta 200 ESEM (FEI Co. Ltd, Cambridge, England) in low vacuum mode, i.e. samples were not coated with gold and examined in the native state. A similar setup was used at the company (AstraZeneca) for initial evaluation of the crystallisation behaviour of the system and for the investigation of the heuristic temperature cycling approach. An in situ Lasentec in-process video PVM700^{TM} microscope (Mettler Toledo, Leicester, UK) was used to monitor crystal size and shape changes in the crystal slurries.

3. Results and discussion

3.1. In situ ATR-UV–vis calibration model development

A calibration model was developed for concentration determination using ATR-UV–vis spectroscopy. Calibration experiments were performed at three saturation temperatures 20 °C, 30 °C and 40 °C. During these experiments the system was monitored by FBRM and ATR-UV–vis spectroscopy. The data were recorded at various temperatures to include both undersaturated and supersaturated regions. The temperature, total count/s and absorbance profile at 259 nm are shown in Fig. 3. In all calibration experiments temperature was raised 10 °C above the saturation temperature and the lower temperature limit was 10 °C or until nucleation occurred. Clear and cloud points were determined using FBRM results accompanied by ATR-UV–vis data. Principal components regression (PCR) was used to develop a calibration model. PCR is a well-established multivariate calibration method and uses principal component analysis (PCA) and least squares regression (Brereton, 2003; Keithley et al., 2009; Massart et al., 1998; Næs et al., 2002). Raw absorbance, first and second derivative spectra of AZD7009 are shown in Fig. 4. To determine which form of spectral pre-processing should be used, PCR models using each spectral pre-processing were developed. A PCR model using second derivative with five principal components was selected as it gave the best results with a root mean square prediction error of less than 3% between actual and measured concentrations. It should be noted that the application of partial least squares (PLS) calibration model has also been investigated and for this particular system, there was very little difference in the predictions from PCR and PLS. This was because the main chemical component detectable in the UV spectral range used for this work was the API, with very minor spectral contributions from the solvents. Therefore, most of the variance observed in the spectral data was very highly correlated to the concentration of API and the associated temperature effects. Consequently, the primary principal components obtained by the PCA decomposition step in PCR were all highly correlated to the analyte concentration and therefore PCR performed as well as PLS using the same number of factors.

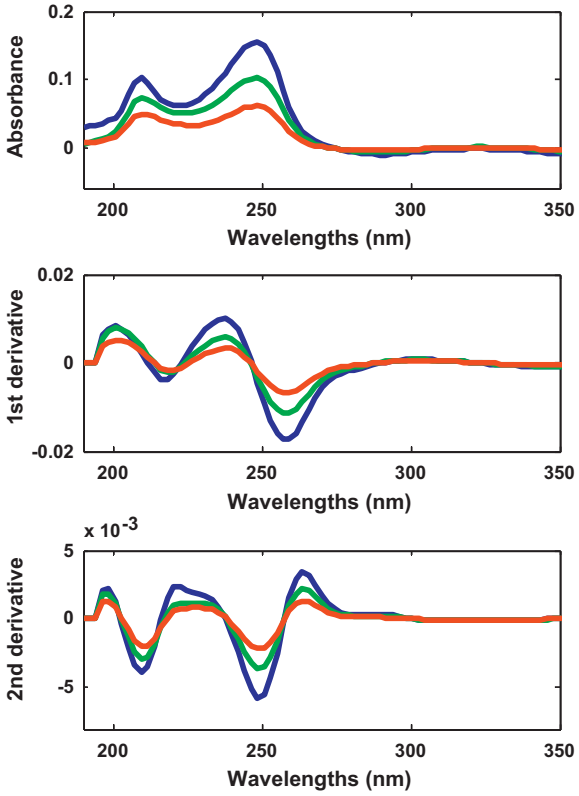

Fig. 4. Raw absorbance, first and second derivatives of the AZD7009 comppound at different concentrations and temperatures.

The key difficulties with the crystallization of this compound were the solvent inclusion and the formation of small agglomerated particles. The agglomeration was evident by PVM images obtained by AstraZeneca during the development phase of AZD7009 and showed that the crystals consisted of agglomerates of needle-shaped crystals (Fig. 5). Agglomeration has been shown to be a function of supersaturation, i.e. agglomeration is faster at high supersaturation and the agglomerates formed become harder to break up (Simons et al., 2004; Brunsteiner et al., 2005).

Since the product was not a solvate, it was hypothesized that solvent inclusions could be the cause of the DIPE smell. There are three main ways solvent can be associated with a solid, i.e. on the surface when it is incompletely dried, as a solvate (or clathrate) or through liquid inclusions (Zhang and Grant, 2005). As noted by

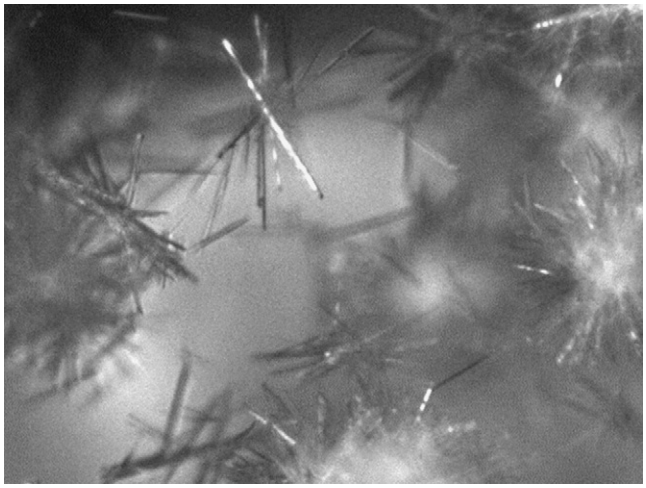

Fig. 5. PVM image of AZD7009 agglomerates in the crystallization solvent.

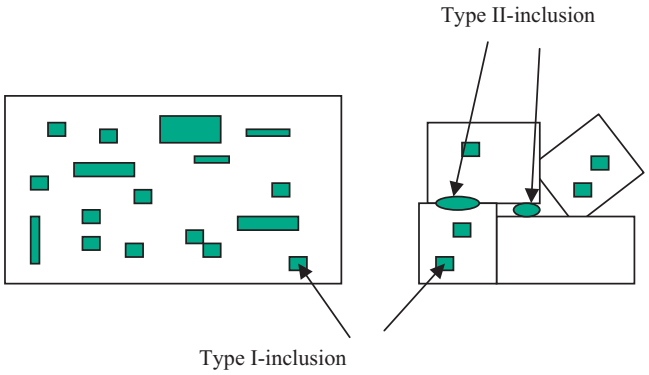

Fig. 6. Type I and Type II solvent inclusions (after Saito et al. (2001).

Dumas et al. (2002), there are three types of primary solvent inclusion: (i) small inclusions which arise due to unstable growth, (ii) channels of separate inclusions, due to the growth step not being straight, but globe-like, and (iii) large layers that arise since there is critical height for a straight step beyond which a layer of solution is trapped.

Saito et al. (2001) have defined two types of solvent inclusion, i.e. Type I and II (Fig. 6). Type I inclusions are those that are included within the crystal and is the result of unstable growth (Mullin, 2001). Type II inclusions, on the other hand, lie between the agglomerated crystals. Examination of the crystal agglomerates by SEM after isolation and drying showed no evidence of Type I inclusions on the surface of the crystals and hence the cause of the residual smell of DIPE was thought to be due to Type II inclusions of the solvent in the agglomerate, i.e. the DIPE was trapped between the crystals.

To test the strength of the agglomerates a sample was placed on a microscope slide and suspended in silicone oil. This caused the agglomerates to disperse to some degree and when covered with a glass slip and sheared slightly they were disrupted even further. In this respect, they can be classified as 'soft' agglomerates, in contrast to hard agglomerates, which require considerably more shear to disrupt the cemented crystals (Nichols et al., 2002). Some agglomerates did remain intact, which yielded a suspension of hard and soft agglomerates and many primary crystals.

Agglomeration can also occur during the drying process whereby at the early stages of drying there is solvent in the pores and spaces between neighbouring crystals. This can give rise to capillary effects that tend to pull the crystals together and predispose them to agglomeration and solvent inclusion: the tendency to agglomerate during the drying process will be exacerbated if the crystal size is small (Lekhal et al., 2004).

SEM was used to examine the agglomerates in more detail and Fig. 7(b) shows low (×241) and Fig. 7(a) high magnification (×2394) SEM images of an agglomerate obtained after drying. The SEMs showed no evidence of Type I inclusions and hence the cause of the residual smell of DIPE is most likely due to Type II solvent inclusions.

3.2. Automated direct nucleation control experiments

In order to address the issues of solvent inclusion and obtain larger AZD7009 crystals, automated direct nucleation control (ADNC) was applied. ADNC is a model free feedback control approach using information from FBRM (Saleemi et al., 2012a,b). Direct nucleation control approach has been shown to generate larger, uniform crystals with minimal agglomeration (Abu Bakar et al., 2009a,b; Saleemi et al., 2012a). ADNC is a flexible and sophisticated method of maintaining the number of particles at the desired level. Apart from selecting the desired target counts, upper and lower limits for target counts along with temperature limits and heating/cooling rates can also be specified based on the system dynamics. The upper and lower limits on the target counts/s are required to eliminate unnecessary frequent switching between the cooling and heating phases, and/or account for potential slow drift in signal due to change in shape of particles. The bounds for the counts/s are chosen by the user, however statistical control charts could be used to provide an alternative way of differentiating noise in the FBRM measurement from the changes caused by real nucleation/dissolution events (Simon et al., 2010a,b). ADNC varies the

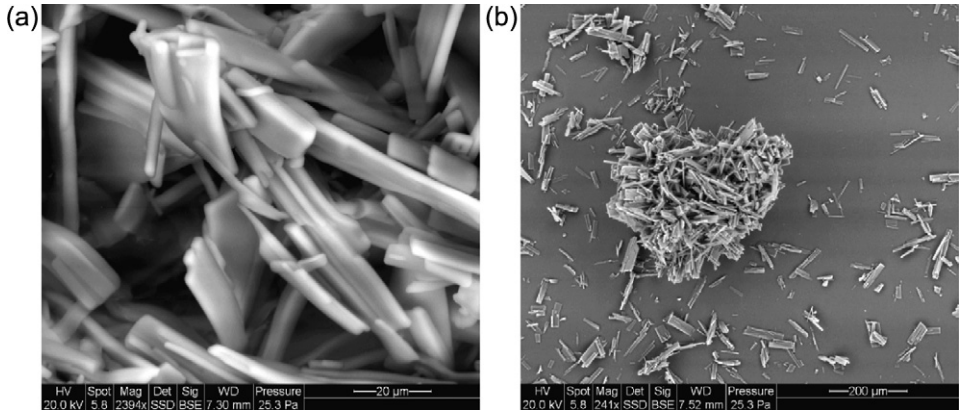

Fig. 7. SEM images AZD7009 after drying in a vacuum oven (a) high magnification (×2394) and (b) low magnification (×241).

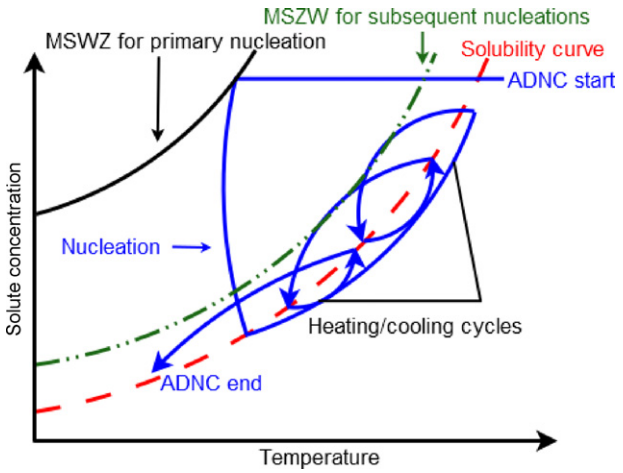

Fig. 8. Schematic working of ADNC approach.

process temperature to keep the number of particles at the setpoint. As a result of these temperature cycles, fines are continuously dissolved whilst maintaining a certain number of counts. Since the smaller crystals have a larger surface area compared to the larger crystals they will preferentially dissolve on heating. On cooling, the supersaturation generated by the dissolution of the small crystals is then deposited on the remaining crystals and hence the average particle size of the crystals in the slurry increases. Schematic working of the ADNC approach is shown in Fig. 8. The process starts once complete dissolution has taken place. Cooling continues until the unset of nucleation. When the upper limit of the target counts/s is exceeded the system switches to heating and tries to bring the FBRM counts/s to the setpoint. During the heating phase the operating curve goes below the solubility curve resulting in dissolution of crystals. Once the setpoint has been attained the operating curve returns again into the supersaturated region. During this phase the supersaturation generated by the dissolution of the smaller particles is consumed by the crystals present in the slurry resulting in their growth. These cycles continue until the process reaches the setpoint limit along with the target counts.

The effect of these heating/cooling cycles on the crystals is shown in Fig. 9. Temperature cycling, apart from growth of the crystals, also assists agglomerate disruption and, consequently any solvent trapped between the agglomerates will be released. These results are in accordance with the literature where it has been shown that temperature cycling helps in removal of solvent inclusion and increases crystal size (Kim et al., 2003, 2011). Note that the temperature cycles also help in the elimination of Type I solvent inclusions, since the repeated heating cooling cycles lead to repeated surface dissolution and regrowth of the faces of the larger crystals at low supersaturation, yielding the elimination of solvent molecules incorporated in the crystal structure during growth.

Unlike typical temperature cycling which is applied by a trial and error method, ADNC determines automatically the number of cycles, heating and cooling rates and the moment when switching between heating and cooling should occur. ADNC can be readily applied to most crystallisation systems using the CryPRINS software. Note that although in principle other sensor that provide a signal that is a continuous function of the particle concentration, (e.g. low cost turbidity, or bulk video imaging) can be used for the implementation of the ANDC approach, the advantage of the FBRM is that the counts/s signal is relatively independent (or has a much weaker dependence compared to other sensors) on the growth of particles. However since the drift in signal due to growth is generally slower and smaller compared to the changes due to nucleation/dissolution this disadvantage can be minimized by appropriate implementation of the ADNC approach, which takes into account the rate and magnitude of change in the signal to identify true nucleation/dissolution events (Saleemi et al., 2012a,b). The ADNC approach exploits the benefits of controlled dissolution to achieve better product properties, which otherwise can only be obtained using more complicated model-based control and optimisation approaches (Nagy, 2009; Nagy et al., 2011, 2008a,b).

3.3. Comparison between ADNC and linear cooling runs

In order to compare the efficiency of ADNC, an unseeded linear cooling experiment was also performed. The concentration of the solute used in these experiments was 0.065 g/g, and the total duration of the run was kept the same. The total counts/s, concentration and temperature profiles for both runs are shown in Fig. 10.

Based on a previous trial run carried out to understand the dynamics of the process, an ADNC experiment was conducted where the target counts were set at 8000 counts/s with upper and lower limits of ±1000 counts/s. The ADNC approach was initiated once complete dissolution occurred. Three heating/cooling cycles (with maximum rates of ±0.2 °C/min) were required before the target counts were reached and the process stabilized at the lower process temperature limit of 10 °C. Variations in total counts/s and concentration profiles as a result of temperature cycling generated by ADNC can be seen in Fig. 10(a). In the case of linear cooling, the total counts/s remained approximately constant after nucleation took place until the end (Fig. 10(b)). The onset of nucleation occurred at high supersaturation therefore a large number of small nuclei were generated and the supersaturation decreased close to the equilibrium concentration. Further cooling the system at a slow rate (0.03 °C/min) kept the supersaturation at very small values ensuring that the system was growth dominated. The concentration can be seen to be constantly decreasing, since the supersaturation was used up by the generation of a very large number of small particles resulting in a small change in the square weighted chord length distribution (SWCLD) of the crystals (Fig. 11(a)). For the linear run SWCLD indicates very small growth throughout the run (Fig. 11(b)). SWCLD can be used qualitatively

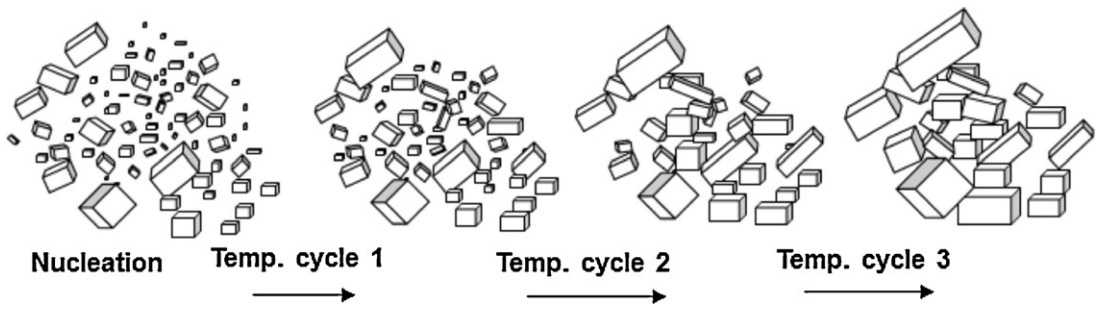

Fig. 9. Effect of temperature cycling on a crystal suspension.

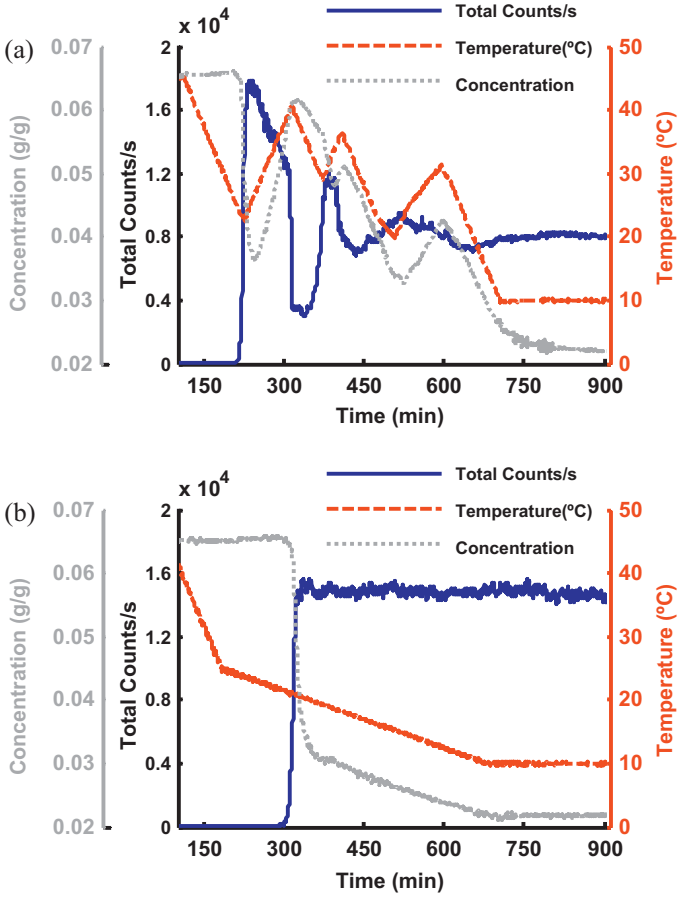

Fig. 10. Total counts/s, concentration and temperature profiles for (a) ADNC run (b) linear cooling run.

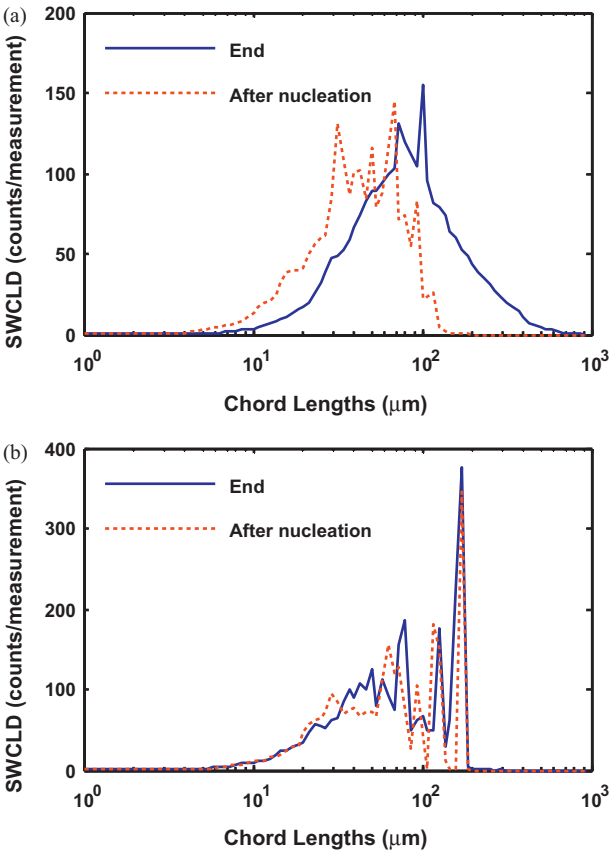

Fig. 11. Square weighted chord length distribution (SWCLD) for the (a) ADNC run and (b) linear cooling run.

to indicate any changes in crystal size because of agglomeration or growth.

The SWCLD for the ADNC run indicates significant growth in the system as can be seen by the shift in the distribution towards a larger chord length. The difference in SWCLD for both profiles can be clearly seen in Fig. 12(a). In addition, the evolution of square weighted mean chord length (SWMCL) shows continuous growth during ADNC run, whereas the profile for the linear run indicates much less growth in the system.

Whilst for the implementation of the ADNC approach concentration measurement is not required, using the calibrated ATR-UV–vis spectroscope to monitor the process allows evaluation of the ADNC operating curve in the phase diagram providing a better understanding of the crystallization process. The data collected during the ADNC run starting from the completely dissolved solution when the ADNC was started is shown in Fig. 13. As shown previously, three heating/cooling cycles were required to produce the large crystals. The figure also illustrates that during the heating phases the concentration consistently moves along the same operating line, which corresponds closely to the solubility curve of the compound. Hence during the ADNC cycles the solubility curve is also automatically determined in situ. This ability to determine the solubility curve is helpful in case there is a shift because of, e.g. the presence of impurities or as a result of different crystal size. The ADNC approach also automatically adjusts the operating curve to the changes in the nucleation curve. As illustrated in Fig. 13, the first (primary) nucleation occurs at a higher supersaturation, yielding to a larger dissolution cycle, whereas the second and third cycles occur at much lower supersaturation values since solid is already present

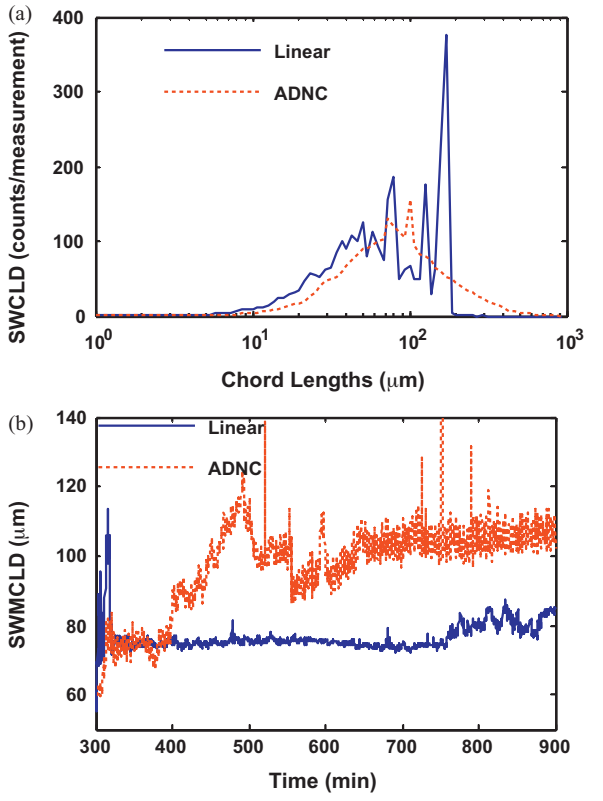

Fig. 12. (a) Comparison of the SWCLD for the ADNC and linear runs at the end of the batch and (b) evolution of SWMCL for the ADNC and linear runs.

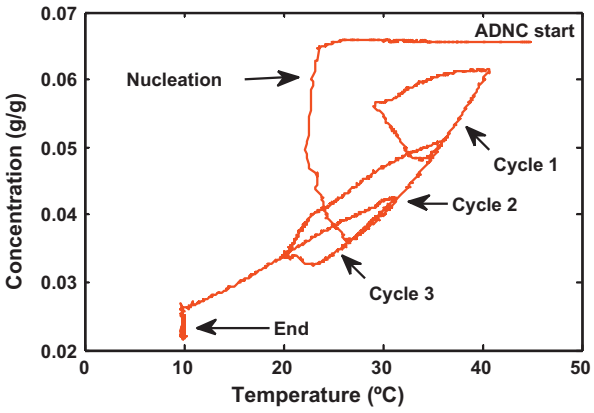

Fig. 13. Phase diagram for the ADNC run.

in the system. These results demonstrate the completely adaptive feature of the ADNC approach.

Similar, albeit uncontrolled temperature cycling experiments were initially performed at the company to eliminate the problems related to agglomeration and solvent inclusion.

After several trial-and-error experimental optimisations of the ripening conditions and economic evaluation based on operating costs, three temperature cycles (similar to the ADNC experiment) and a batch time of approximately 9 h were confirmed as the optimal operating conditions. The PVM images recorded during the three temperature cycles demonstrate that the cycles rectified agglomeration, as shown in Fig. 14. These images show that agglomerated crystals were obtained after the onset of primary nucleation, but as the process proceeded the dissolution steps during the temperature cycling dissolves the bonds between the particles and eliminates the agglomerates. At the same time crystals also increased considerably in size. The DNC approach determined completely automatically that three cycles are needed to obtain the best crystal quality, resulting in a batch time of approximately 9 h, results which coincide with the optimal number of cycles and batch time determined within the company based on economic considerations and trial-and-error optimisation.

In case of the linear cooling experiment the crystals remained in agglomerated form throughout the process. The crystals obtained from the ADNC run when analysed showed negligible amount of DIPE.

Optical microscopy and SEM images of the product from both batches are significantly different as shown in Figs. 15 and 16. The crystals from ADNC batch are larger, with well-defined shapes, with less breakage and agglomeration. The product obtained from the linear run mainly consists of small broken crystals with large lumps of aggregated particles. Experimental investigation demonstrated that larger crystals of the API have better flow and compression characteristics; hence the application of the ADNC in addition to eliminating problems related to solvent inclusion can yield better tablets. Some preliminary seeding experiments (40 °C) were also undertaken and found to be viable alternative to temperature cycling to avoiding crystallization induced agglomeration. However, with respect to seeding, Ressler (1997) has noted that seeding could create significant amounts of paperwork and, therefore, inconvenience to production personnel since records must be maintained so that seed material can be traced to origin to comply with current good manufacturing processes (cGMP) practice. Additionally, the production of seed with consistent quality is often difficult and the variation in the seeds can translate into large variability in the product properties. In contrast, the ADNC approach

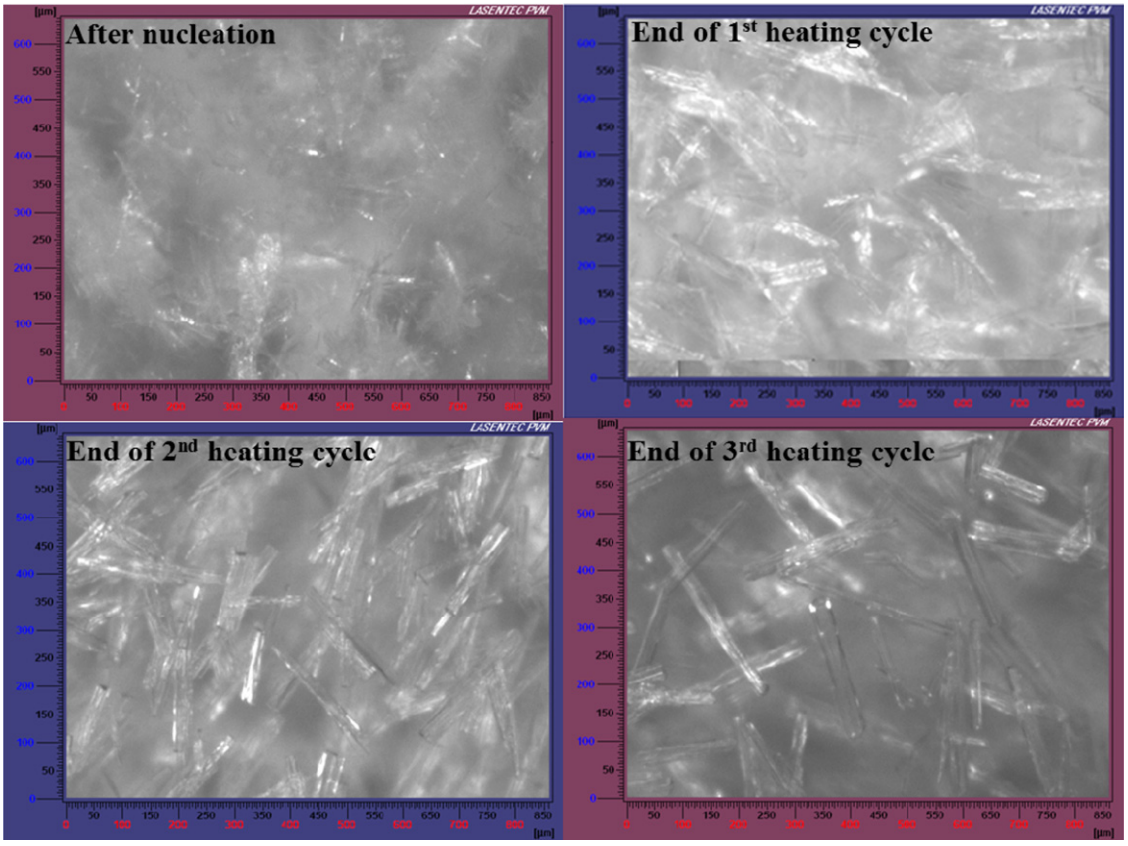

Fig. 14. PVM images showing growth and de-agglomeration of crystals during the three cycles of a temperature cycling experiment.

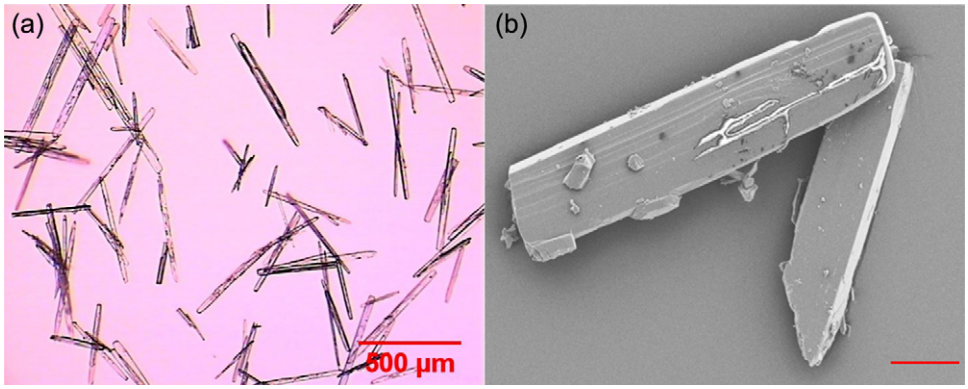

Fig. 15. Product images obtained at the end of the ADNC run (a) optical microscope image (b) SEM image (scale bar equals 20 μm).

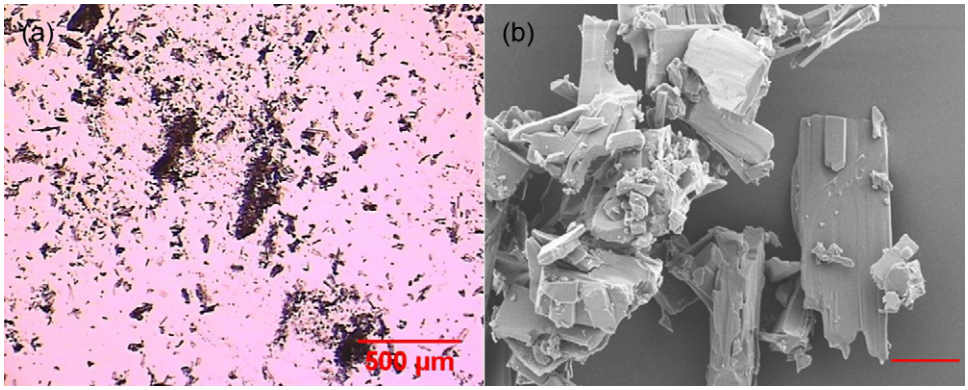

Fig. 16. Product images obtained at the end of the linear cooling run (a) optical microscope image (b) SEM image (scale bar equals 20 μm).

can produce in situ consistent seed and react to any change in the quality of the seed, shift in metastable zone, or other process disturbances such as accidental seeding, from crust formed on the wall (Mersmann, 1988; Saleemi et al., 2012a).

4. Conclusions

The automated direct nucleation control (ADNC) approach has been shown as a successful crystallization control method which was able to produce large, high quality crystals of the cardiovascular drug, AZD7009, eliminating production problems due to agglomeration and hence solvent inclusion. The effects of the automated temperature cycles were to de-agglomerate the particles, thus eliminate solvent inclusion (reducing the residual smell of di-*iso*-propylether) and to promote growth, yielding crystals with better flow and compression characteristics. The ADNC control approach is completely automated, hence it is much easier to implement than a trial and error based temperature cycling method. A direct comparison with linear cooling profile showed that the ADNC approach resulted in product of superior quality in terms of crystal size distribution, and agglomeration, which can provide better final product characteristics when making extended release tablets.

Acknowledgements

Financial support is acknowledged by the European Research Council under the European Union's Seventh Framework Programme (FP7/2007+2013)/ERC grant agreement no. (280106+CrySys). AstraZeneca R&D Charnwood, Loughborough is acknowledged for supplying AZD7009 and technical support.

References

Aamir, E., Nagy, Z.K., Rielly, C.D., 2010a. Optimal seed recipe design for crystal size distribution control for batch cooling crystallisation processes. Chem. Eng. Sci. 65, 3602–3614.
Aamir, E., Nagy, Z.K., Rielly, C.D., 2010b. Evaluation of the effect of seed preparation method on the product crystal size distribution for batch cooling crystallization processes. Cryst. Growth Des. 10, 4728–4740.
Abu Bakar, M.R., Nagy, Z.K., Rielly, C.D., 2009a. Seeded batch cooling crystallization with temperature cycling for the control of size uniformity and polymorphic purity of sulfathiazole crystals. Org. Process Res. Dev. 13, 1343–1356.
Abu Bakar, M.R., Nagy, Z.K., Saleemi, A.N., Rielly, C.D., 2009b. The impact of direct nucleation control on crystal size distribution in pharmaceutical crystallization processes. Cryst. Growth Des. 9, 1378–1384.
Abu Bakar, M.R., Nagy, Z.K., Rielly, C.D., 2010. Investigation of the effect of temperature cycling on surface features of sulfathiazole crystals during seeded batch cooling crystallization. Cryst. Growth Des. 10, 3892–3900.
Abu Bakar, M.R., Nagy, Z.K., Rielly, C.D., Dann, S.E., 2011. Investigation of the riddle of sulfathiazole polymorphism. Int. J. Pharm. 414, 86–103.
Barrett, P., Smith, B., Worlitschek, J., Bracken, V., O'Sullivan, B., O'Grady, D., 2005. A review of the use of process analytical technology for the understanding and optimization of production batch crystallization processes. Org. Process Res. Dev. 9, 348–355.
Barthe, S., Rousseau, R.W., 2006. Utilization of focused beam reflectance measurement in the control of crystal size distribution in a batch cooled crystallizer. Chem. Eng. Technol. 29, 206–211.
Billeter, J., Neuhold, Y., Simon, L., Puxty, G., Hungerbühler, K., 2008. Uncertainties and error propagation in kinetic hard-modelling of spectroscopic data. Chemom. Intell. Lab. Syst. 93, 120–131.
Billot, P., Couty, M., Hosek, P., 2010. Application of ATR-UV spectroscopy for monitoring the crystallisation of UV absorbing and nonabsorbing molecules. Org. Process Res. Dev. 14, 511–523.
Borissova, A., Khan, S., Mahmud, T., Roberts, K.J., Andrews, J., Dallin, P., Chen, Z., Morris, J., 2009. In situ measurement of solution concentration during the batch cooling crystallization of L-glutamic acid using ATR-FTIR spectroscopy coupled with chemometrics. Cryst. Growth Des. 9, 692–706.
Brereton, R.G., 2003. Chemometrics: Data Analysis for the Laboratory and Chemical Plant. John Wiley & Sons, Chichester, England.
Brunsteiner, M., Jones, A.G., Pratola, F., Price, S.L., Simons, S.J.R., 2005. Toward a molecular understanding of crystal agglomeration. Cryst. Growth Des. 5, 3–16.

Camarasu, C., Madichie, C., Williams, R., 2006. Recent progress in the determination of volatile impurities in pharmaceuticals. TrAC Trends Anal. Chem. 25, 768–777.
Deneau, E., Steele, G., 2005. An in-line study of oiling out and crystallization. Org. Process Res. Dev. 9, 943–950.
Doki, N., Seki, H., Takano, K., Asatani, H., Yokota, M., Kubota, N., 2004. Process control of seeded batch cooling crystallization of the metastable-form glycine using an in situ ATR-FTIR spectrometer and an in situ FBRM particle counter. Cryst. Growth Des. 4, 949–953.
Dumas, M., Carvin, P., Biscans, B., 2002. Characterization of liquid inclusions formed in industrial organic crystal. Chem. Eng. Trans. 2, 713–718.
Fujiwara, M., Chow, P.S., Ma, D.L., Braatz, R.D., 2002. Paracetamol crystallization using laser backscattering and ATR-FTIR spectroscopy: metastability, agglomeration, and control. Cryst. Growth Des. 2, 363–370.
Goldstein, R.N., Khrestian, C., Carlsson, L., Waldo, A.L., 2004. A new antiarrhythmic drug with predominant effects on the atria effectively terminates and prevents reinduction of atrial fibrillation and flutter in the sterile pericarditis model. J. Cardiovasc. Electrophysiol. 15, 1444–1450.
Hagsten, A., Casper Larsen, C., Møller Sonnergaard, J., Rantanen, J., Hovgaard, L., 2008. Identifying sources of batch to batch variation in processability. Powder Technol. 183, 213–219.
Hermanto, M.W., Chow, P.S., Tan, R.B.H., 2010. Implementation of focused beam reflectance measurement (FBRM) in antisolvent crystallization to achieve consistent product quality. Cryst. Growth Des. 10, 3668–3674.
Hishamuddin, E., Stapley, A.G.F., Nagy, Z.K., 2011. Application of laser backscattering for monitoring of palm oil crystallisation from melt. J. Cryst. Growth 335, 172–180.
Howard, K.S., Nagy, Z.K., Saha, B., Robertson, A.L., Steele, G., 2009a. Combined PAT-solid state analytical approach for the detection and study of sodium benzoate hydrate. Org. Process Res. Dev. 13 (3), 590–597.
Howard, K.S., Nagy, Z.K., Saha, B., Robertson, A.L., Steele, G., Martin, D., 2009b. A process analytical technology based investigation of the polymorphic transformations during the anti-solvent crystallization of sodium benzoate from IPA/water mixture. Cryst. Growth Des. 9, 3964–3975.
Hunter, W., Downing, J., 1949. The peroxidation of diethyl ether and di-iso propyl ether. J. Soc. Chem. Ind. 68, 362–364.
Jia, C., Yin, Q., Zhang, M., Wang, J., Shen, Z., 2008. Polymorphic transformation of pravastatin sodium monitored using combined online FBRM and PVM. Org. Process Res. Dev. 12, 1223–1228.
Juppo, A., Steele, G., 2006. Preparation of crystalline N,N'-disubstituted oxabispidines and their use as cardiovascular agents. PCT Int. Appl. WO 2006/137772 A1.
Kail, N., Marquardt, W., Briesen, H., 2009. Process analysis by means of focused beam reflectance measurements. Ind. Eng. Chem. Res. 48, 2936–2946.
Keithley, R.B., Mark Wightman, R., Heien, M.L., 2009. Multivariate concentration determination using principal component regression with residual analysis. TrAC Trends Anal. Chem. 28, 1127–1136.
Kim, S., Wei, C., Kiang, S., 2003. Crystallization process development of an active pharmaceutical ingredient and particle engineering via the use of ultrasonics and temperature cycling. Org. Process Res. Dev. 7, 997–1001.
Kim, J., Kim, J., Kim, H., Koo, K., 2011. Application of internal seeding and temperature cycling for reduction of liquid inclusion in the crystallization of RDX. Org. Process Res. Dev. 15, 602–609.
Lekhal, A., Girard, K.P., Brown, M.A., Kiang, S., Khinast, J.G., Glasser, B.J., 2004. The effect of agitated drying on the morphology of L-threonine (needle-like) crystals. Int. J. Pharm. 270, 263–277.
Li, R.F., Penchev, R., Ramachandran, V., Roberts, K.J., Wang, X.Z., Tweedie, R.J., Prior, A., Gerritsen, J.W., Hugen, F.M., 2008. Particle shape characterisation via image analysis: from laboratory studies to in-process measurements using an in situ particle viewer system. Org. Process Res. Dev. 12, 837–849.
Massart, D.L., Vandeginste, B.G.M., Buydens, L.M.C., Jong, S.D., Lewi, P.J., Smeyers-Verbeke, J., 1998. Handbook of Chemometrics and Qualimetrics. Elsevier Science B.V, Amsterdam, The Netherlands.
Mersmann, A., 1988. Design of crystallizers. Chem. Eng. Process. 23, 213–228.
Mullin, J.W., 2001. Crystallization, fourth ed. Butterworth-Heinemann, Oxford, UK.
Næs, T., Isaksson, T., Fearn, T., Davies, T., 2002. A User-Friendly Guide to Multivariate Calibration and Classification. NIR Publications, Chichester, England.
Nagy, Z.K., 2009. Model based robust control approach for batch crystallization product design. Comput. Chem. Eng. 33, 1685–1691.
Nagy, Z.K., Chew, J.W., Fujiwara, M., Braatz, R.D., 2008a. Comparative performance of concentration and temperature controlled crystallizations. J. Process Contr. 18 (3–4), 399–407.
Nagy, Z.K., Fujiwara, M., Braatz, R.D., 2008b. Modelling and control of combined cooling and anti-solvent crystallization processes. J. Process Contr. 18, 856–864.
Nagy, Z.K., Aamir, E., Rielly, C.D., 2011. Internal fines removal using a population balance model based control of crystal size distribution under dissolution, growth and nucleation mechanisms. Cryst. Growth Des. 11, 2205–2219.
Nichols, G., Byard, S., Bloxham, M.J., Botterill, J., Dawson, N.J., Dennis, A., Diart, V., North, N.C., Sherwood, J.D., 2002. A review of the terms agglomerate and aggregate with a recommendation for nomenclature used in powder and particle characterization. J. Pharm. Sci. 91, 2103–2109.
Qu, H., Louhi-Kultanen, M., Rantanen, J., Kallas, J., 2006. Solvent-mediated phase transformation kinetics of an anhydrate/hydrate system. Cryst. Growth Des. 6, 2053–2060.
Ressler, R., 1997. Batch crystallization – a good solution to tough solids problems. Pharmaceutical Engineering 17, 43–46.
Saito, N., Yokota, M., Fujiwara, T., Kubota, N., 2001. A note of the purity of crystals produced in batch suspension crystallization. Chem. Eng. J. 84, 573–575.
Saleemi, A., Rielly, C., Nagy, Z.K., 2012a. Automated direct nucleation control for in situ dynamic fines removal in batch cooling crystallization. CrystEngComm. 14, 2196–2203.
Saleemi, A.N., Rielly, C.D., Nagy, Z.K., 2012b. Comparative investigation of supersaturation and automated direct nucleation control of crystal size distributions using ATR-UV/Vis spectroscopy and FBRM. Cryst. Growth Des., doi:10.1021/cg201269c.
Saleemi, A.N., Rielly, C.D., Nagy, Z.K., 2012c. Monitoring of the combined cooling and antisolvent crystallization of mixtures of aminobenzoic acid isomers using ATR-UV/Vis spectroscopy and FBRM. Chem. Eng. Sci., doi:10.1016/j.ces.2012.02.005.
Simon, L.L., Myerson, A.S., 2011. Continuous antisolvent plug-flow crystallization of a fast growing API. In: Proceedings of the 18th International Symposium on Industrial Crystallization (ISIC 18), September 13–16, Zurich, Switzerland.
Simon, L.L., Nagy, Z.K., Hungerbuhler, K., 2009a. Endoscopy-based in situ bulk video imaging of batch crystallization processes. Org. Process Res. Dev. 13, 1254–1261.
Simon, L.L., Nagy, Z.K., Hungerbuhler, K., 2009b. Comparison of external bulk video imaging with focused beam reflectance measurement and ultra-violet visible spectroscopy for metastable zone identification in food and pharmaceutical crystallization processes. Chem. Eng. Sci. 64, 3344–3351.
Simon, L.L., Oucherif, K.A., Nagy, Z.K., Hungerbuhler, K., 2010a. Bulk video imaging based multivariate image analysis, process control chart and acoustic signal assisted nucleation detection. Chem. Eng. Sci. 65, 4983–4995.
Simon, L.L., Oucherif, K.A., Nagy, Z.K., Hungerbuhler, K., 2010b. Histogram matching, hypothesis testing, and statistical control-chart-assisted nucleation detection using bulk video imaging for optimal switching between nucleation and seed conditioning steps. Ind. Eng. Chem. Res. 49, 9932–9944.
Simons, S.J.R., Pratola, F., Jones, A., Brunsteiner, G., Price, M.S.L., 2004. Towards a fundamental understanding of the mechanics of crystal agglomeration: a microscopic and molecular approach. Part. Part. Syst. Char. 21, 276–283.
Smallwood, I.M.N., 2002. Solvent Recovery Handbook. Blackwell Science Ltd., Oxford, UK.
Variankaval, N., Cote, A.S., Doherty, M.F., 2008. From form to function: crystallization of active pharmaceutical ingredients. AIChE J. 54, 1682–1688.
Yu, L.X., Lionberger, R.A., Raw, A.S., D'Costa, R., Wu, H., Hussain, A.S., 2004. Applications of process analytical technology to crystallization processes. Adv. Drug Deliv. Rev. 56, 349–369.
Zhang, G.G.Z., Grant, D.J.W., 2005. Formation of liquid inclusions in adipic acid crystals during recrystallization from aqueous solutions. Cryst. Growth Des. 5, 319–324.